Received: 8 May 2024 | Revised: 14 August 2024 | Accepted: 15 August 2024

DOI: 10.1002/pc.28993

RESEARCH ARTICLE

Polymer COMPOSITES WILEY

An experimental study on the wear performance of 3D printed polylactic acid and carbon fiber reinforced polylactic acid parts: Effect of infill rate and water absorption time

Berkay Ergene[1] | **Yiğit Emre İnci**[1] | **Batuhan Çetintaş**[2] | **Birol Daysal**[1]

[1]Faculty of Technology, Mechanical Enginering Department, Pamukkale University, Denizli, Turkey

[2]Faculty of Engineering, Mechanical Engineering Department, Pamukkale University, Denizli, Turkey

Correspondence
Berkay Ergene, Faculty of Technology, Mechanical Enginering Department, Pamukkale University, Denizli, Turkey.
Email: bergene@pau.edu.tr

Funding information
Tubitak 2209A Project, Grant/Award Number: 1919B012220430

Abstract

Rapid prototyping, also known as additive manufacturing, is a nascent technology that is gaining traction in the context of environmental concerns and waste reduction, as well as the growing trend towards customized design. The additive manufacturing method, which has applications in diverse fields such as aviation, architecture, biomedical and automotive engineering, has also begun to be utilized in the construction of yachts and yacht hulls within the maritime industry. In this experimental study, the influences of sea water on polylactic acid (PLA) and carbon fiber reinforced polylactic acid (PLA/CF) parts manufactured at different infill rates (20%, 60% and 100%) were investigated. The parts were exposed to sea water for three different periods (1, 5, and 10 days) and subsequently subjected to wear tests. The dimensional accuracy, surface roughness, hardness, water absorption, volume loss, and friction coefficient of parts were measured and calculated. Additionally, the worn surfaces of the parts were investigated using field emission scanning electron microscope (FESEM) images. The findings indicate that PLA and PLA/CF parts can be produced with high dimensional accuracy. Furthermore, it can be reported that the water absorption of PLA/CF parts increased, particularly with an increase in the infill rate, while the volume loss decreased. Obtained results indicate the necessity of optimizing the 3D printing parameters and the relationship between the ambient conditions and the wear performance of the 3D printed parts.

Highlights

- 3D printing is a highly promising method for the production of polymer composites.
- A pioneering study into the effect of infill rate and water absorption on the wear performance.

- Coefficient of friction values of PLA and PLA/CF parts ranged between 0.37 and 0.75.
- PLA/CF mostly exhibited higher volume loss than PLA with water absorption.
- Volume loss declines with a raise in the infill rate from 20% to 100%.

KEYWORDS

3D printing, infill rate, PLA/CF, water absorption, wear performance

1 | INTRODUCTION

The industry's demand for the simple production of lightweight components with intricate geometries is stimulating interest in novel materials and production methods. 3D printing technology, which was first commercially utilized by Charles Hull in 1987, is a production method that functions by adding material layer upon layer to achieve the desired final geometry of the product. Therefore, additive manufacturing (AM) differs from conventional production methods such as forging, milling, turning, or casting.[1–4] AM is regarded as a highly preferred manufacturing method in the industry, largely due to its capacity to produce parts from a wide variety of materials, including ceramics, metals, plastics, and composite materials. Additionally, the complex geometry of the produced parts, minimal post-production processes, and minimal material waste have contributed to its growing popularity.[5–9] Due to its superior manufacturing properties, AM is widely preferred in many areas such as automotive, aviation, architecture, biomedical, sport, and marine. Crash boxes and bumpers in automotive,[10] aircraft parts in aerospace,[11] personalized implants and scaffolds in biomedical,[12] fast produced bridges and buildings with complex geometries in architecture,[13] airless basketball[14] and shoes with lattice cores[15] in sport and lastly surfboards[16] and yachts in marine[17] exhibit the widespreading of this technology in the global world. Although AM technology is divided into seven main classes, including vat-photopolymerization, binder jetting, material jetting, material extrusion, powder bed fusion, direct energy deposition, and laminated object manufacturing, according to the ISO 52900 and ASTM F2792 standards, it can be stated that fused filament fabrication (FFF) stands out among the seven methods because of the ease of availability of materials and spare parts, the simplicity of device use, and the low cost.[18–20]

FFF enables the fabrication of a variety of polymers, including PLA, acrylonitrile butadiene styrene (ABS), polyamide (PA), polyethylene terephthalate glycol (PETG), polyether ether ketone (PEEK), as well as carbon or glass fiber reinforced polymers.[21–25] In this method, the product is created in advance and its three-dimensional design is sliced in a suitable slicing program. The product is then heated to the melting temperature of the filament and the filament is deposited on the manufacturing table according to the determined g-code. This process is repeated until the three-dimensional product is obtained.[26]

PLA filaments which are biodegradable preferred due to their superior physical properties, including ease of processing due to low melting points, alloyability, sufficient viscosity and high stiffness.[27–29] In addition to these properties, the shape memory effect is a significant physical property of PLA that has recently attracted the attention of several research groups.[30,31] Fiber-reinforced PLA composites, which are formed by combining PLA material with carbon or glass fiber reinforcements, exhibit high strength at low weight and improved combined material properties. In the context of marine applications where composite materials are utilized in significant quantities, it is evident that watercraft, submarines, offshore parts besides to other marine structural components must cope with the associated environmental challenges. Fiber-reinforced composite materials play a crucial role in the marine field, particularly in the protection against the abrasive and corrosive effects of seawater and in limiting maintenance and repair operations. Fiber-reinforced polymers have been a mainstay of the marine industry since their initial application following the World War II.[32–34] Their introduction was driven by the need to overcome corrosion problems occured with steel, aluminum, and wood. Furthermore, the AM of fiber-reinforced polymer composite parts allows for the weight and design of functional parts to be adjusted as desired, as well as for the creation of customized designs.

A review of the literature reveals that numerous studies have been conducted on the mechanical behaviors of PLA and fiber-reinforced PLA composites manufactured by FFF technology.[35–40] In their study, Dou et al.[35] investigated the impact of various FFF parameters, including layer height, extrusion width, printing speed, and temperature, on the tensile properties of carbon fiber-reinforced PLA (PLA/CF) parts. Their findings indicated

that an increase in layer height, extrusion width, and printing speed resulted in a decline in tensile strength, while a rise in printing temperature had the opposite effect. In another study, Bochnia et al.[36] compared the mechanical properties of thin walled PLA and PLA/CF composites and reported that tensile properties of these materials are affected by the printing orientation parameter. Parallel to this study, Rarani et al.[37] examined a study on the mechanical properties of PLA and PLA/CF composites by applying tensile and three point bending tests. Furthermore, Gavali et al.[38] performed a study on the influence of carbon fiber ratio (12%, 15% and 20%) in the PLA/CF composites on the tensile strength. In conclusion, the results demonstrated that specimens comprising 15% carbon fiber exhibited a 32% enhancement in tensile strength when compared to pure PLA specimens. Besides, Kamaal et al.[39] focused on the optimization of FFF parameters such as layer height, infill rate and building direction on the tensile strength of the PLA/CF parts. Lastly, El Magri et al.[40] pointed out that PLA/CF parts exhibited higher tensile strength than PLA parts and optimum nozzle temperature was found to be 230°C for both PLA and carbon fiber reinforced PLA parts.

Although limited in number, there are studies in the literature that examine the wear performance of PLA and PLA/CF parts. As an illustration, the research team led by Srinivasan et al.[41] conducted an investigation to assess the influence of infill ratio, infill pattern, and layer height on the wear performance of PLA/CF. Based on the findings of their experimental work, they concluded that a raise in infill rate enhances wear strength, while an increase in layer height leads to a reduction in wear rate. Additionally, they demonstrated that layer height can be considered as the most influential parameter in determining wear strength. Furthermore, Mohamed et al.[42] investigated the influence of production parameters on the coefficient of friction for FFF-manufactured parts. They employed scanning electron microscopy (SEM) to obtain micrographs, which revealed that thick layers were associated with the formation of fractures, cracks, and deep grooves, ultimately affecting friction properties. What's more, Al Abir et al.[43] demonstrated that the addition of carbon fiber and graphene nanoparticles into the PLA improved the wear resistance of the part fabricated with FFF. In addition, Hanon and Zsidai[44] made a research on the effects of filament color and printing orientation on the wear performance of 3D printed PLA samples. Conclusionly, Şirin et al.[45] aimed to determine the influence of infill rate on the friction coefficient of 3D printed PLA parts and they claimed that PLA parts with infill rate of 50% displayed superior wear resistance in comparison with PLA parts with infill rate of 30% and 70%.

TABLE 1 FFF parameters of the manufactured test samples.

Parameter	PLA	PLA/CF
Layer height (mm)	0.2	
Infill rate (%)	20, 60, 100	
Infill pattern	Line	
Printing speed (mm/s)	40	
Fan speed (%)	100	
Building orientation	Vertical	
Raster angle (°)	0/90	
Support structure	None	
Adhesion type	Skirt	
Number of contour	3	
Building platform temperature (°C)	60	
Nozzle temperature (°C)	210	230

As previously stated, a limited number of researches have been performed on the mechanical and wear properties of PLA and PLA/CF parts manufactured with FFF. However, there is currently no study on the wear performance of PLA and PLA/CF parts produced with FFF and exposed to seawater. In this experimental study, the influences of seawater exposure on PLA and PLA/CF parts produced with FFF at different infill rates (20%, 60% and 100%) were investigated for the first time. The parts were subjected to wear test after being exposed to seawater for various periods of time (1, 5, and 10 days). In addition to the outcomes of wear tests, such as friction coefficient and mass loss, surface roughness, hardness, and macroscopic, microscopic, and FESEM observations were conducted to determine the surface defects and wear tracks.

2 | MATERIALS AND METHODS

In this study, pin on disc wear test specimens with the diameter of 10 mm and height of 20 mm were designed in Solidworks 2023 designing program according to ASTM G99.[46] After the designing procedure, the CAD file in the stl format was imported into the Ultimaker Cura 5.6.0 slicing program and FFF parameters were assigned as tabulated in Table 1. As illustrated in Table 1, three different infill rate values of 20%, 60% and 100% were applied and they can be seen in Figure 1 with details. In addition, obtained g-code file was transferred to the MY3B Z23 3D printer via Syrox Micro SD card and 3D printing was performed by using PLA filament (Flashforge) and carbon reinforced PLA filament (Flashforge). Furthermore, material properties of the used

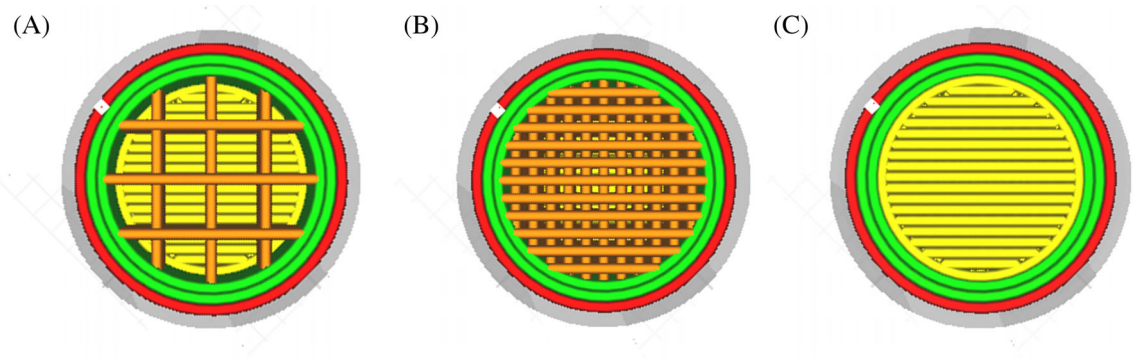

FIGURE 1 An illustration from the slicer program showing the infill rates of the samples produced, (A) 20%, (B) 60%, (C) 100%.

TABLE 2 Material properties of the used PLA and PLA/CF filaments.[47]

Property	PLA	PLA/CF
Density (g/cm^3)	1.20	1.23
Printing temperature (°C)	190–220	200–230
Tensile strength (MPa)	50	55
Young modulus (MPa)	1500	2240
Elongation at break (%)	6	4.8

filaments were shared in Table 2 below according to supplier information.[47]

After the 3D printing process, all samples were controlled with an optical microscope (Nikon SMZ 800 (Tokyo, Japan)) cooperates with Dpx View software in micro-scale to detect whether there is any production problem or not. As a result of controlling, no production based problem was observed and then dimensions of the samples were measured by using an electronic caliper (Asimeto) to determine the dimensional accuracy of the 3D printed parts. What's more, surface roughness of the samples was measured with a surface profilometer (Mahr MarSurf PS1). Additionally, Shore D hardness of the samples was also measured by a durometer (Duroironic model 1000). Lastly, weight of the each sample was measured with a precision balance (Radwag AS/220/C/2) before putting the samples into the sea water athmosphere with different durations (1, 5 and 10 days) to determine their water absorption ability. Once again, the precision balance was utilized for calculating the final weights of the samples, so the mass increment after water absorption could be calculated.

To employee the wear tests of the 3D printed samples, a pin on disc wear test machine (Turkyus Podwt) was used. During the wear tests, a sand paper with mesh size of 320 grid was preferred as counterpart which has speed of 2 m/s. In addition, test load of 10 N was applied to the samples for 90 s. Force and time datas were recorded with Esit Data Logger 1.1.8 software during the wear tests and then force datas were used to calculate the coefficient of friction of the samples via Equation (1). Furthermore, the mass loss of the samples was quantified by weighing the samples before and after the wear tests. The calculated mass loss was then divided by the density of the samples to obtain the volume loss of the samples (Equation 2). Moreover, worn surfaces were imaged with a Zeiss (Gemini) FESEM as shown with details in Figure 2. Lastly, melting temperatures and glass transition temperatures of the additively manufactured PLA and PLA/CF samples were determined by using differential scanning calorimeter (DSC) (DSC 131 EVO) and dynamic mechanic analyses (DMA) (DMA 242 E Artemis).

$$\text{Coefficient of friction} = \frac{\text{Frictional force}\,(N)}{\text{Normal force}\,(N)} \quad (1)$$

$$\text{Volume loss}\,(\text{mm}^3) = \frac{\text{Mass loss}\,(g)}{\text{Density}\,(g/\text{mm}^3)} \quad (2)$$

3 | RESULTS AND DISCUSSIONS

3.1 | Dimensional accuracy, surface roughness, DSC and DMA analyses

Additive manufacturing, a preferred method for the production of industrial products, allows for the creation of lightweight components with intricate geometries. However, it is also crucial to produce parts that closely adhere to the original design specifications, both in terms of the final product and the assembly of the parts. It is established that lightweight and high-dimensional accuracy parts can be produced using the material extrusion-based FFF method. In Table 3, dimensional accuracy of the wear samples were given depending on the material and

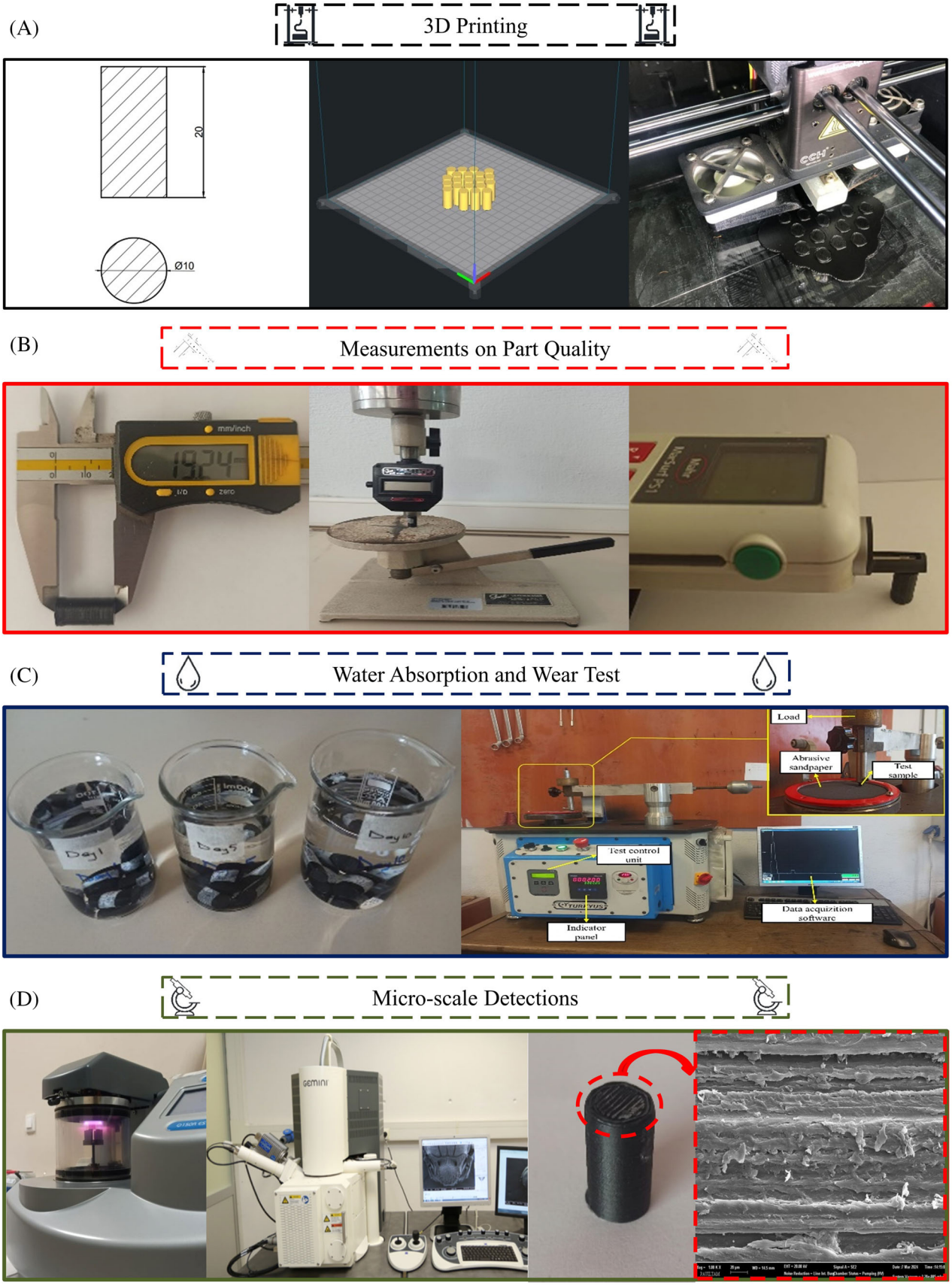

FIGURE 2 Work flow diagram of the applied measurement, test and observations, (A) 3D printing process, (B) Mesurements, (C) Water absorption and wear test, (D) Micro-scale detections.

infill rate. According to Table 3, maximum dimensional accuracy in height of 96.43% with standard deviation (SD) (SD:0.184%) and maximum dimensional accuracy in diameter of 99.51% (SD:0.395%) were calculated for the PLA samples with infill rate of 20% and 100% respectively. For the PLA/CF samples, the peakest dimensional accuracies in height and diameter of 98.98% (SD:0.150%) and 97.12% (SD:0.539%) were observed at the samples manufactured with infill rate in order of 100% and 20%. Besides, it is worth to express that height of the PLA/CF samples were measured higher than the nominal CAD height although it is not valid for PLA samples. It is believed that this outcome may stem from the presence of the carbon fibers in the composite sample. Lastly, it can be pointed out that PLA samples exhibited higher dimensional accuracy in diameter of the samples. On the other hand PLA/CF samples showed higher dimensional accuracy in height of the samples. Parallel results to findings of this study was also found in the effort of Hanon et al.[48] who focused on the influence of the FFF parameters and filament color on the dimensional accuracy of the parts manufactured with FFF technology. As an outcome of their work, it was announced that dimensional accuracy in the height of the sample ranged between % 98.36 ile % 99.72. Besides, the dimensional accuracy in diameter was found to be fluctuating between % 98.45 and % 99.63. What's more, the dimensional accuracy of the PA6, PA6/CF and PA6/GF was calculated between % 98.40 and % 99.86 in another study.[49]

Figure 3 illustrates the surface roughness results of PLA and PLA/CF parts fabricated at varying infill rate values. The data presented in Figure 3 indicates that PLA/CF parts exhibit higher surface roughness than PLA parts. Additionally, the surface roughness values for PLA/CF parts demonstrate an increasing trend with increasing infill rate. However, this increasing trend is not observed for PLA parts, where the surface roughness of PLA parts decreases smoothly with increasing infill rate. The peakest surface roughness value of 10.2 μm (SD: 2.4 μm) and the lowest surface roughness value of 4 μm (SD: 0.3 μm) were observed for the PLA/CF sample with a 100% infill rate and the PLA sample with a 100% infill rate, respectively. Similar observations were also

TABLE 3 Dimensional accuracy of the 3D printed samples.

Material	Infill rate (%)	Average height (mm)	Nominal height (mm)	Accuracy in height (%)	Average diameter (mm)	Nominal diameter (mm)	Accuracy in diameter (%)
PLA	20	19.28 (SD:0.036)	20	96.43 (SD:0.184)	9.93 (SD:0.039)	10	99.35 (SD:0.398)
	60	19.26 (SD:0.037)		96.31 (SD:0.185)	9.94 (SD:0.028)		99.41 (SD:0.288)
	100	19.24 (SD:0.039)		96.23 (SD:0.195)	9.95 (SD:0.039)		99.51 (SD:0.395)
PLA/CF	20	20.23 (SD:0.015)		98.84 (SD:0.078)	9.71 (SD:0.053)		97.12 (SD:0.539)
	60	20.25 (SD:0.018)		98.73 (SD:0.090)	9.63 (SD:0.060)		96.39 (SD:0.604)
	100	20.20 (SD:0.030)		98.98 (SD:0.150)	9.54 (SD:0.072)		95.42 (SD:0.727)

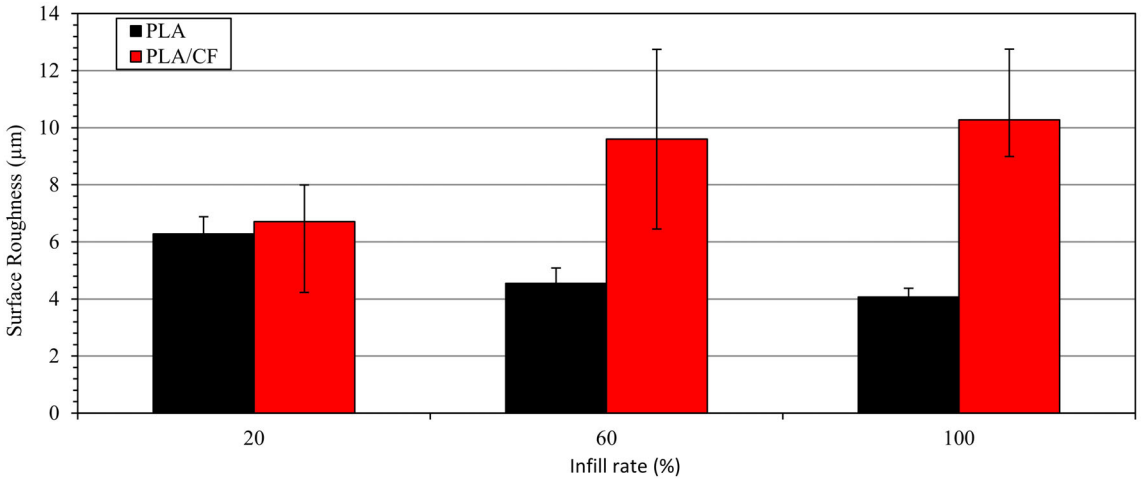

FIGURE 3 Measured surface roughness values of the samples.

reported in other literature efforts. For instance, Jain et al.[50] examined the impact of infill rate on the surface roughness of PLA parts, including those with a 0.2 mm layer thickness produced via FFF technology. Their findings indicated that rising the infill rate up from 20% to 100% resulted in a reduction in surface roughness value from 5.4 to 1.93 μm. In another study,[51] it was claimed that an addition of carbon fiber into the polymer matrix lead to an increase in surface roughness of the 3D printed part.

DSC analysis was conducted to ascertain the melting temperature values of the 3D-printed samples. Figure 4 depicts the DSC curves of the manufactured samples, indicating that the PLA and PLA/CF samples exhibit melting temperatures of 170.8 and 149.7°C, respectively. The term glass transition temperature can be defined as the temperature at which a rigid polymeric sample undergoes a transformation, becoming a more flexible and viscous material. This critical temperature is typically determined through DMA applications based on gradual increases in test temperatures. In this study, to estimate approximate glass transition temperatures, tanδ results collected after DMA were used to identify easily distinguishable peak values. Figure 5 illustrates the tanδ peak values of the fabricated samples with varying analysis temperatures, indicating that the glass transition temperatures are 73.3°C for PLA and 72.7°C for PLA/CF samples.

3.2 | Water absorption and hardness of the samples

Due to the nature of FFF, which is a layer-based production method, pores can occur in the produced parts. In addition, the effect of different FFF parameters such as infill rate and whether the filament used is fiber reinforced or not are also known to affect the porosity of the produced parts. In this context, the water absorption of the PLA and PLA/CF parts produced at different infill rates at various time periods is presented in Figure 6. In

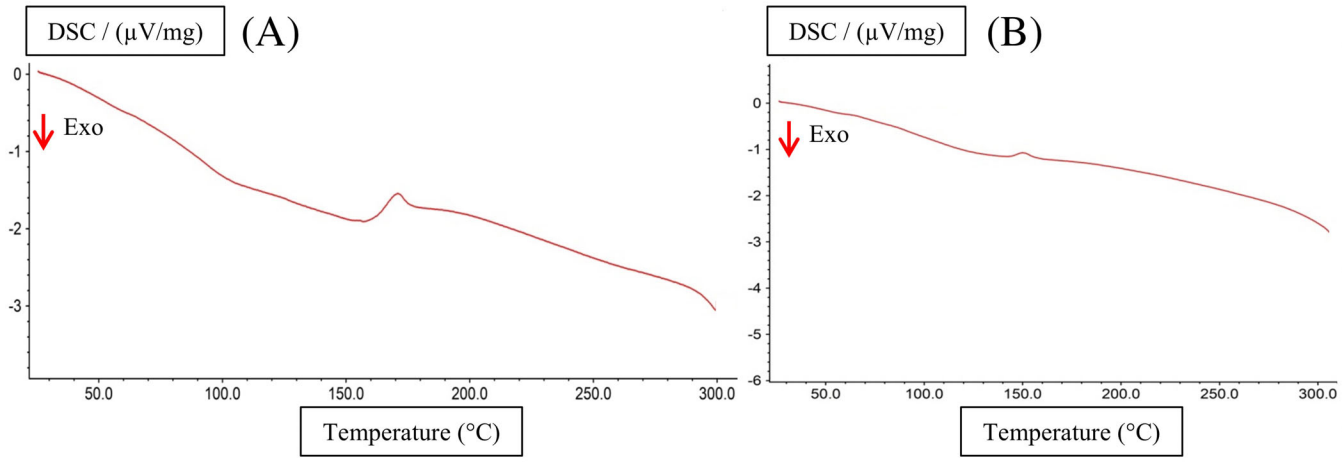

FIGURE 4 DSC curves of the addivitely manufactured samples, (A) PLA, (B) PLA/CF.

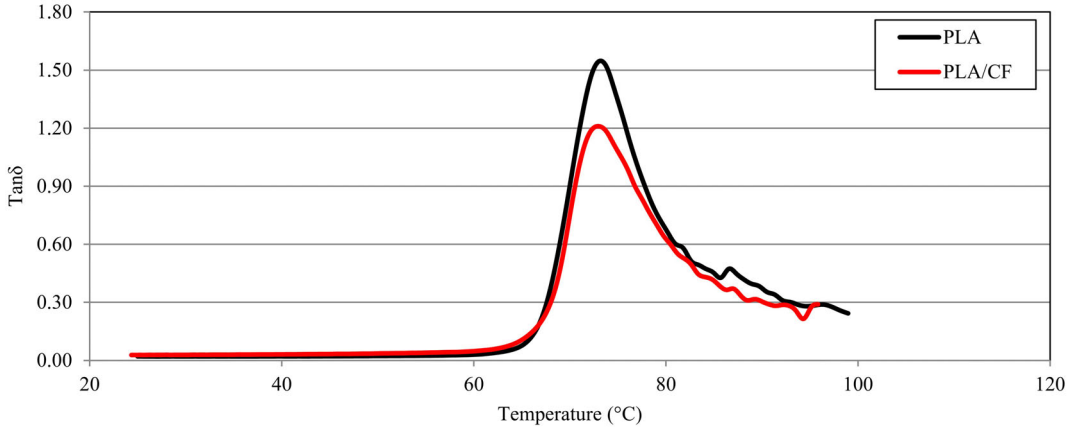

FIGURE 5 DMA-based tanδ graph of the additively manufactured samples.

order to ascertain the water absorption of the components, the given Equation (3) was employed.

$$\text{Water absorption}\,(\%) = \frac{M_a - M_b}{M_b} \times 100 \qquad (3)$$

where, M_b and M_a demonstrate the mass of the samples before and after water absorption respectively. Upon evaluation of Figure 6, it can be concluded that there is no direct correlation between the duration of the samples in the water environment and the amount of water absorbed by the products. This outcome is compatible with the results of other researches in the literature.[52,53] Moreover, PLA/CF parts exhibit a higher degree of water absorption than PLA parts. This phenomenon becomes more pronounced when the infill rate of the parts is increased from 20% to 100%. It is well-established that the diffusion of water molecules in polymeric composites is influenced by three principal mechanisms.[54] The initial one pertains to the diffusion of water molecules into the micro-cracks that may be found within the polymer matrix. The second mechanism is based on the transport

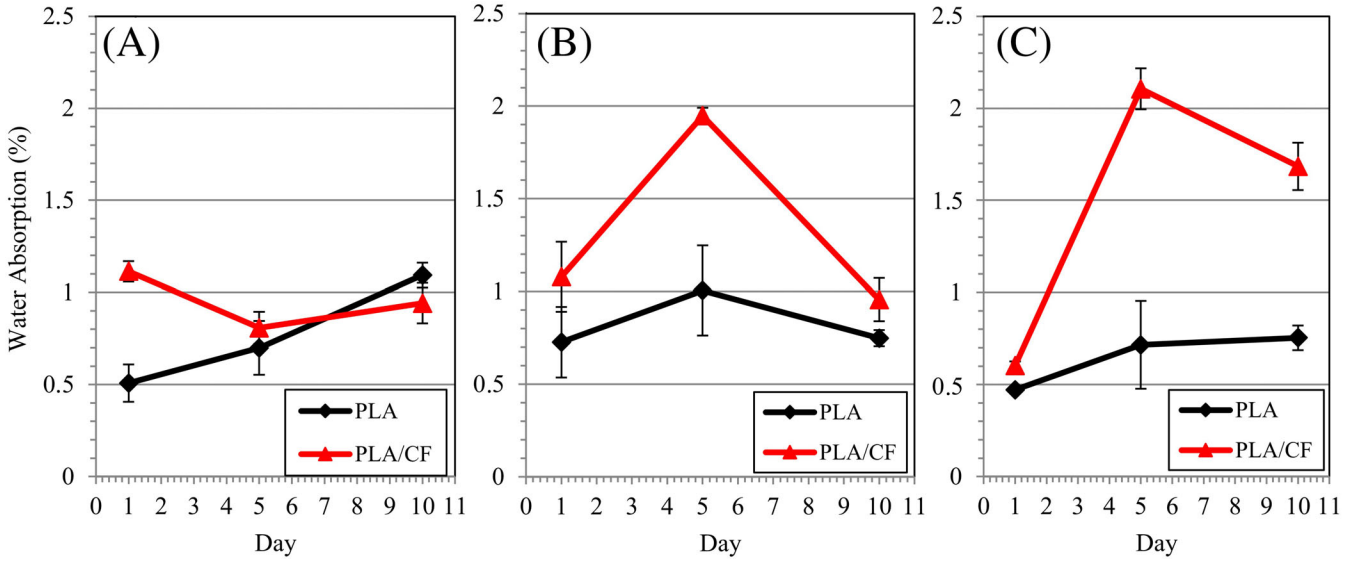

FIGURE 6 Water absorption of the PLA and PLA/CF parts manufactured with different infill rates depending on various time periods, (A) 20%, (B) 60% and (C) 100%.

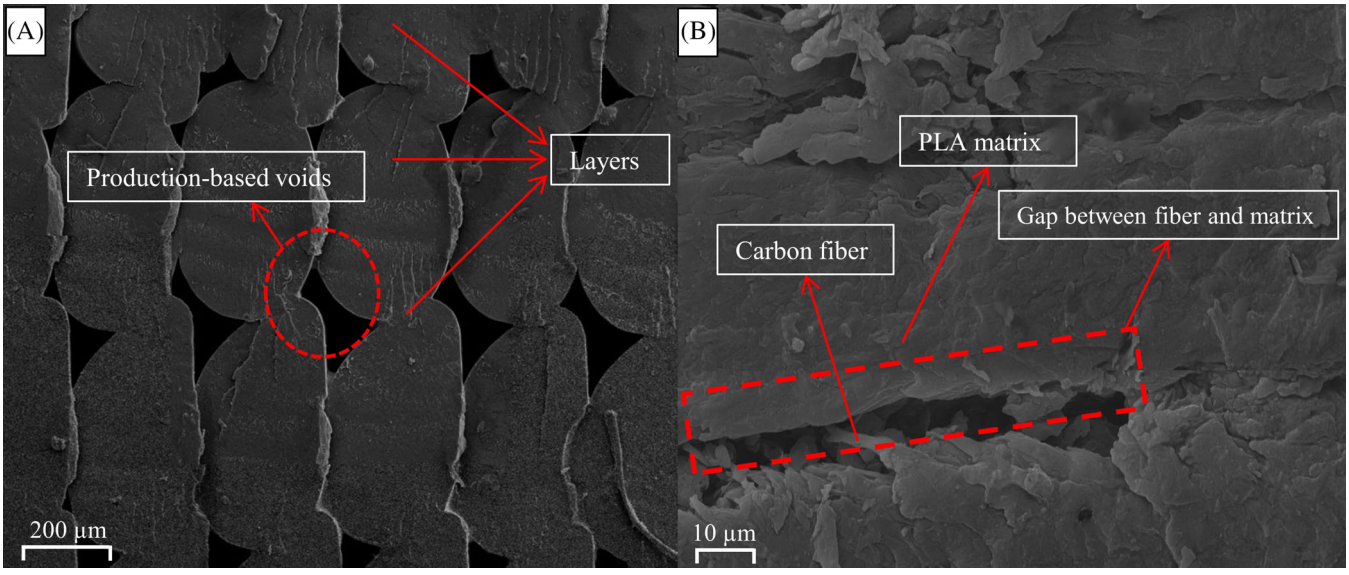

FIGURE 7 Potential water absorption zones in 3D printed parts, (A) production-based voids, (B) gap between fiber and matrix interface.

of water molecules into the interfacial spaces between the fibers and the polymer matrix. The third mechanism refers to the diffusion of water molecules through microcracks that may be present in the polymer matrix structure. These all factors may affect the water absorption of the PLA/CF. Moreover, Figure 7 depicts the presence of voids and gaps between the fibers and the PLA, which are the result of production processes, and which serve to facilitate the penetration of water. Furthermore, Guo et al.[55] conducted a study on the impact of fiber composition on the water absorption capacity of composites based on polymers. Their findings indicated that the presence of carbon fiber or a raise in carbon fiber content in the composite led to an increment in water absorption. Moreover, the water absorption of the PLA parts ranged from 0.47% to 1.09%. These results fluctuated between 0.60% and 2.10% for the PLA/CF parts. Besides, Chandran et al.[56] investigated the water absorption and its effects on the mechanical properties of the 3D printed and compression molded PLA parts. As a finding of their study, it was stated that 3D printed samples exhibited higher water absorption than compression molded samples due to the higher level of porosity in the 3D printed parts. It is also worth to express that they have also observed a sharp increase in water absorption up to 100 h, and then low increase or decrease occured like in this study. Finally, a stabilization in water absorption was reported after 300 h and all this period was related to the Fick's law.

Figure 8A–C show the hardness (Shore D) of the PLA and PLA/CF samples fabricated with 20%, 60% and 100% infill rate under different water absorption times. From Figure 8, it can be observed that the PLA/CF samples showed higher hardness levels than the PLA parts. In addition, the effect of water absorption day on the hardness of the samples showed different effects depending on the material and infill rate. For example, PLA and PLA/CF parts behaved similarly when considering the 20% infill rate. The hardness of the parts first decreased on day 1 and day 5. After that, the hardness of the parts increased and reached the initial hardness level or higher (Figure 8A). By evaluating Figure 8B, it can be said that the water absorbing process caused the hardness of the parts to decrease for both PLA and PLA/CF parts compared to their initial hardness. In addition, a decrease in the hardness of PLA/CF parts with a 100% infill rate was observed as the water absorption time increased. However, the hardness of the PLA parts increased until the 5-day period and then decreased sharply and approached the initial hardness value (Figure 8C). Finally, the Shore D hardness values of the parts vary between 62.3 Shore D (SD: 1.4 Shore D) and 79.1 Shore D (SD: 0.8 Shore D).

3.3 | Volume loss and friction coefficient of worn samples

Figure 9 illustrates the volume loss of PLA and PLA/CF parts produced at varying infill rates as a consequence of wear testing following water absorption periods. According to Figure 9, it can be pointed out that volume loss of the both PLA and PLA/CF parts mostly decrease with the increase of infill rate. Ergene and Bolat[57] also conducted a study investigating the impact of infill rate on the volumet loss of PETG components. Their findings indicated that an increase in infill rate resulted in a drop in volume loss. Moreover, the volume loss of the PLA components is higher than that of the PLA/CF components for an infill rate of 20%. However, this situation is reversed for the infill rate of 60%. In this case, the PLA/CF components lose more volume than the PLA components. Finally, a mixed behavior is observed in the wear process

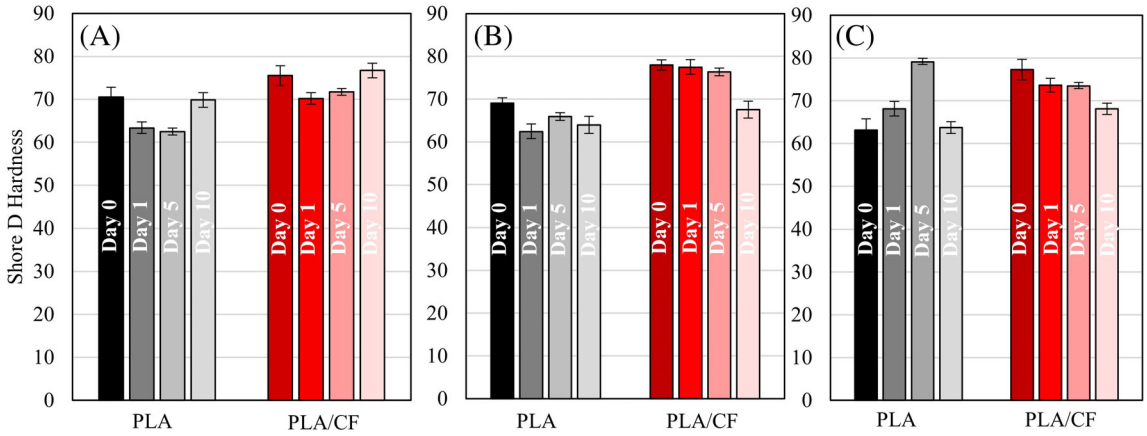

FIGURE 8 Hardness levels of the PLA and PLA/CF parts produced with different infill rates depending on the water absorption period, (A) 20%, (B) 60%, (C) 100%.

of the parts when the infill rate is 100%. Due to the layer-based nature of AM, the infill rate, water absorption mechanism, and the presence of carbon fibers is quite important for the wear performance of the parts and significantly affect the volume loss of the parts. The greatest volume loss, 36.4 mm^3 (SD: 2.2 mm^3), was observed in the PLA component with an infill rate of 20% and subjected to one day of water absorption. Conversely, the lowest volume loss, 15.5 mm^3 (SD:0.86 mm^3), was calculated in the PLA/CF component with an infill rate of 100% and subjected to 10 days of water absorption.

The coefficient of friction of the specimens with different infill rates and subjected to the water absorption process for varying periods during the wear tests are given in Figure 10. The coefficient of friction values exhibited a range of 0.37 (SD:0.07) to 0.75 (SD:0.15) when Figure 10 was taken into consideration. Furthermore, it was observed that PLA parts exhibited higher coefficient of friction values than PLA/CF parts, with the exception of those fabricated with an infill rate of 20% and subjected to 5 days of water absorption. Furthermore, it can put forward that water absorption periods affects the

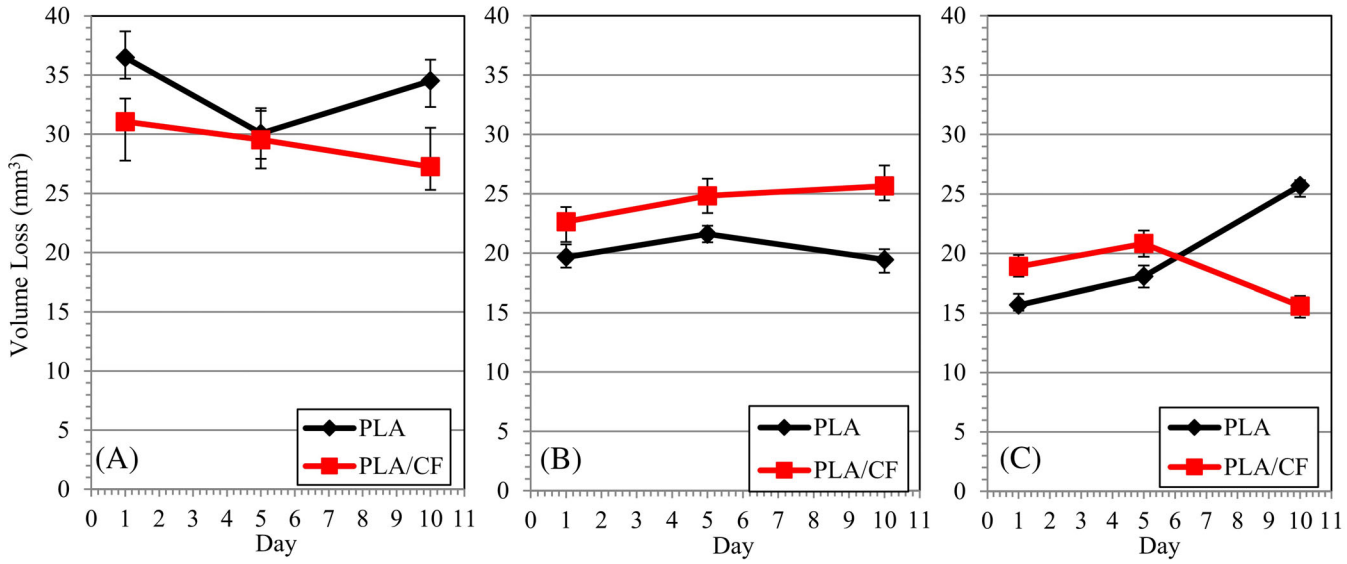

FIGURE 9 Variation of the volume loss of the parts produced with different infill rates and subjected to various water absorption periods, (A) 20%, (B) 60%, (C) 100%.

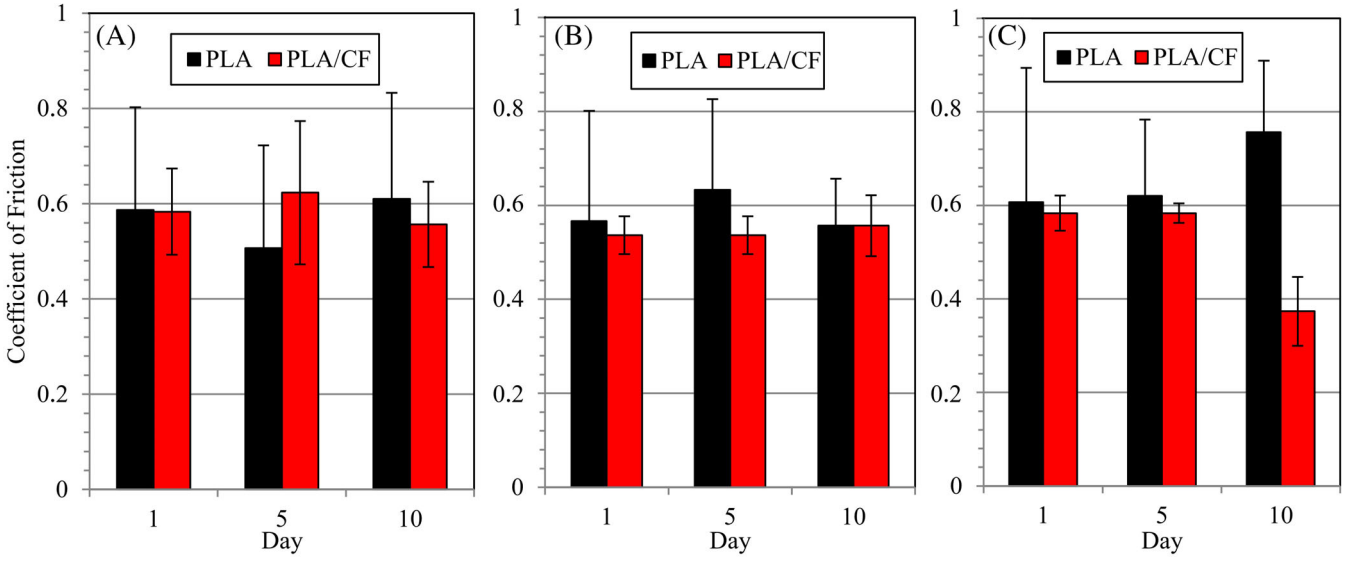

FIGURE 10 Change of coefficient of friction depending on the water absorption period and infill rate, (A) 20%, (B) 60%, (C) 100%.

coefficient of friction of the parts change with their infill rate parameter.

3.4 | Microscopic observations

Figures 11 and 12 illustrate the surfaces of the specimen groups exhibiting the highest and lowest volume loss during the abrasion tests respectively. A comparison of the PLA specimens produced with a infill rate of 20% in Figure 11 and subjected to abrasion testing reveals a notable volume loss, in alignment with the findings presented in Figure 9. The predominant debris particles also corroborate this observation. The discrepancy between the water absorption periods of the first and tenth days is that the minimal level of plastic deformation, which was not discernible at the conclusion of the first day, becoming apparent at the end of the tenth day (Figure 11A,B). Furthermore, the FESEM image of the PLA/CF parts subjected to a wear test after one day of water absorption reveals the presence of adhesive wear zones and deep grooves. Additionally, upon the occurrence of 10 days of water absorption, the formation of small-sized local grooves can be observed, which replace the deep and larger grooves (Figure 11C,D). Figure 12 exhibits the worn surfaces of the samples produced with 100% infill rate. According to Figure 12, low level plastic deformations are observed in PLA samples after 1 day of water

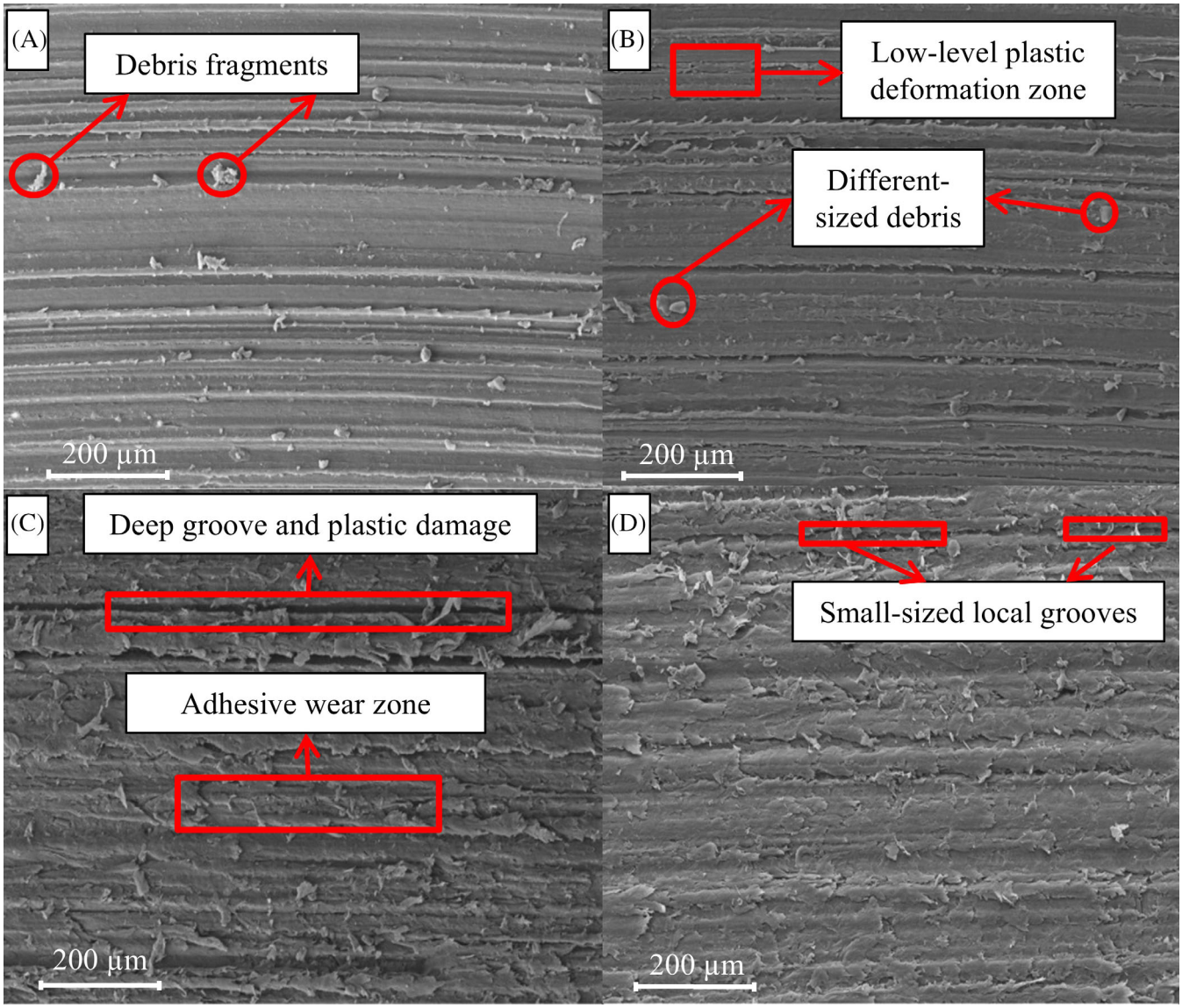

FIGURE 11 FESEM images of PLA and PLA/CF parts produced with 20% infill rate and subjected to wear tests after various water absorption periods, (A) PLA sample after 1 day, (B) PLA sample after 10 day, (C) PLA/CF sample after 1 day, (D) PLA/CF sample after 10 day.

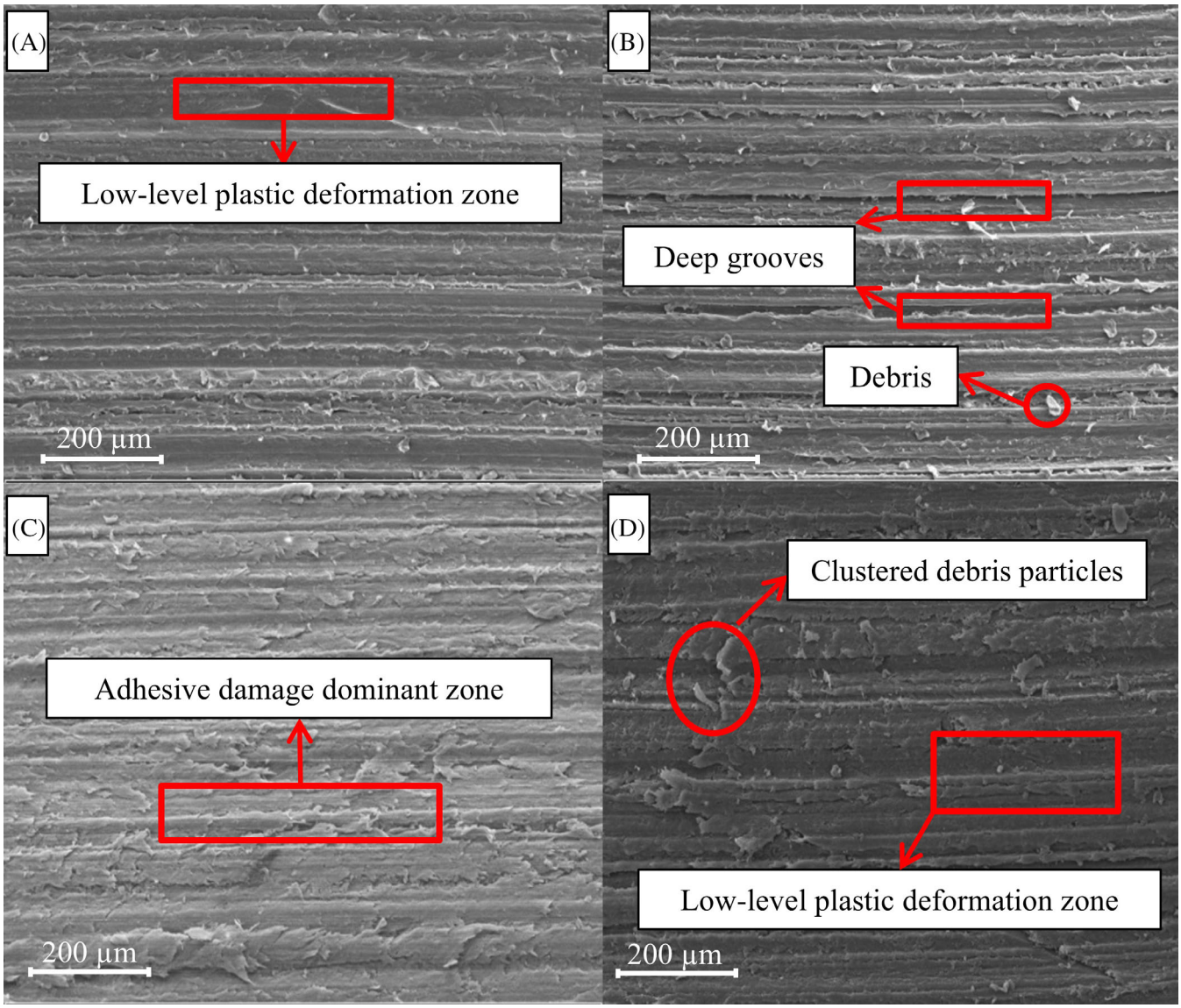

FIGURE 12 FESEM images of PLA and PLA/CF parts produced with 100% infill rate and subjected to wear tests after various water absorption periods, (A) PLA sample after 1 day, (B) PLA sample after 10 day, (C) PLA/CF sample after 1 day, (D) PLA/CF sample after 10 day.

absorption abrasion test, while the presence of deep pits and debris is prominent after 10 days of water absorption abrasion test (Figure 12A,B). In PLA/CF specimens, the adhesive damage dominant zone occurred in the test after 1 day of water absorption, while the test findings after 10 days of water absorption showed clustered debris particles and relatively low plastic deformation zones (Figure 12C,D).

4 | CONCLUSION

The results of this experimental study, which examined the wear test performance of PLA and PLA/CF parts 3D printed with various infill rates in a seawater environment for different periods of time, revealed several important findings. The FFF technology allows for the manufacturing of PLA and PLA/CF parts with high dimensional accuracy levels, which may reach up to 99.51%. The surface roughness of the PLA/CF parts was found to be higher than that of the PLA parts. This may be attributed to the presence of fiber, which has been observed to result in gaps between the interface of the matrix and fiber. Furthermore, it has been demonstrated that PLA/CF parts exhibit a greater capacity for water absorption than PLA parts. This is attributed to the presence of the matrix fiber interface, the enhanced water absorption capacity of the fiber material, and the capillary cracks that form around the fiber. Moreover, as anticipated, the hardness values of the PLA/CF parts

were found to be higher than those of the PLA parts. The volume loss values of PLA and PLA/CF parts exhibited fluctuations in accordance with alterations in the water absorption period and the infill rate of the parts. It can be pointed out that the volume loss value declines with a raise in the infill rate from 20% to 100%. Parallel findings to volume loss results were also obtained for coefficient of friction values of the PLA and PLA/CF parts and they varied between 0.37 and 0.75. Lastly, taken FESEM images from the worn surface of the parts also support the outcomes obtained as a finding of wear tests.

The results of this study demonstrate that the infill rate plays a pivotal role in the water absorption and volume loss of the additively manufactured parts. In addition to examining the effect of infill rate, future studies may also investigate the impact of layer thickness and building direction on the friction properties of produced parts. Furthermore, the effect of coating the produced parts is another area that could benefit from further research. Finally, this study, which presents the results of a wear test conducted on a part in a seawater environment, can be developed by adding abrasive particles to the seawater. This would allow the effect of abrasive conditions in the marine environment to be examined in greater detail.

ACKNOWLEDGMENTS

This study was supported by Tubitak 2209A Project with number of 1919B012220430. Also, the authors would like thank to the CCH Technology and Advanced Technologies Research Center (İLTAM) because of their supports during 3D printing process and FESEM observations respectively.

DATA AVAILABILITY STATEMENT

Data available on request from the authors.

ORCID

Berkay Ergene https://orcid.org/0000-0001-6145-1970
Yiğit Emre İnci https://orcid.org/0009-0006-2915-3256
Batuhan Çetintaş https://orcid.org/0009-0005-9099-7629
Birol Daysal https://orcid.org/0009-0000-0189-4235

REFERENCES

1. Bourell D, Kruth JP, Leu M, et al. Materials for additive manufacturing. *CIRP Ann*. 2017;66(2):659-681. doi:10.1016/j.cirp.2017.05.009
2. Hull CW. The birth of 3D printing. *Res Technol Manag*. 2015;58(6):25-30. doi:10.5437/08956308X5806067
3. Osswald TA, Jack DA, Thompson MS. Polymer composites–special issue review for additive manufacturing of composites. *Polym Compos*. 2023;44(12):8195-8199. doi:10.1002/pc.26631
4. Ravikumar P, Desai C, Kushwah S, Mangrola MH. A review article on FDM process parameters in 3D printing for composite materials. *Mater Today Proc*. 2022;60:2162-2166. doi:10.1016/j.matpr.2021.12.669
5. Tymrak B, Kreiger M, Pearce JM. Mechanical properties of components fabricated with open-source 3D printers under realistic environmental conditions. *Mater Des*. 2014;58:242-246. doi:10.1016/j.matdes.2014.02.038
6. Sugavaneswaran M, Arumaikkannu G. Analytical and experimental investigation on elastic modulus of reinforced additive manufactured structure. *Mater Des*. 2015;66:29-36. doi:10.1016/j.matdes.2014.10.029
7. Bikas H, Stavropoulos P, Chryssolouris G. Additive manufacturing methods and modelling approaches: a critical review. *Int J Adv Manuf Technol*. 2016;83:389-405. doi:10.1007/s00170-015-7576-2
8. Chacón J, Caminero MÁ, García-Plaza E, Núñez P. Additive manufacturing of PLA structures using fused deposition modelling: effect of process parameters on mechanical properties and their optimal selection. *Mater Des*. 2017;124:143-157. doi:10.1016/j.matdes.2017.03.065
9. Domingo M, Puigoriol JM, García AA, Llumà J, Borrós S, Reyes G. Mechanical property characterization and simulation of fused deposition modeling polycarbonate parts. *Mater Des*. 2015;83:670-677. doi:10.1016/j.matdes.2015.06.074
10. Borrelli A, D'Errico G, Borrelli C, Citarella R. Assessment of crash performance of an automotive component made through additive manufacturing. *Appl Sci*. 2020;10(24):9106. doi:10.3390/app10249106
11. Uhlmann E, Kersting R, Klein TB, Cruz MF, Borille AV. Additive manufacturing of titanium alloy for aircraft components. *Procedia CIRP*. 2015;35:55-60. doi:10.1016/j.procir.2015.08.061
12. Chen Y, Li W, Zhang C, Wu Z, Liu J. Recent developments of biomaterials for additive manufacturing of bone scaffolds. *Adv Healthc Mater*. 2020;9(23):2000724. doi:10.1002/adhm.202000724
13. Pajonk A, Prieto A, Blum U, Knaack U. Multi-material additive manufacturing in architecture and construction: a review. *J Build Eng*. 2021;45:103603. doi:10.1016/j.jobe.2021.103603
14. Wilson. The next generation of ball. [Website]. Available from: https://www.wilson.com/en-us/explore/basketball/airless-prototype. Accessed April 12, 2024
15. Mallakpour S, Radfar Z, Hussain CM. *Advanced Application of Additive Manufacturing in the Footwear Industry: from Customized Insoles to Fully 3D-Printed Shoes*. In Medical Additive Manufacturing; Elsevier. 2024;153-178. doi:10.1016/B978-0-323-95383-2.00015-9
16. Forsyth JR, Barnsley G, Amirghasemi M, et al. Understanding the relationship between surfing performance and fin design. *Sci Rep*. 2024;14:8734. doi:10.1038/s41598-024-58387-y
17. Musio-Sale M, Nazzaro PL, Di Nicolantonio M, Rossi E, Alexander T, Peterson E. Visions, concepts, and applications in additive manufacturing for yacht design. Advances in additive manufacturing, modeling systems and 3D prototyping. *AHFE*. 2019;975:401-410. doi:10.1007/978-3-030-20216-3_37
18. ASTM International. *ASTM standard 52900–21*. Additive Manufacturing. General Principles; 2021.
19. Auriemma G, Tommasino C, Falcone G, Esposito T, Sardo C, Aquino RP. Additive manufacturing strategies for personalized drug delivery systems and medical devices: fused filament

fabrication and semi solid extrusion. *Molecules*. 2022;27(9):2784. doi:10.3390/molecules27092784

20. Benfriha K, Ahmadifar M, Shirinbayan M, Tcharkhtchi A. Effect of process parameters on thermal and mechanical properties of polymer-based composites using fused filament fabrication. *Polym Compos*. 2021;42(11):6025-6037. doi:10.1002/pc.26282
21. Vidakis N, Petousis M, Velidakis E, Liebscher M, Mechtcherine V, Tzounis L. On the strain rate sensitivity of fused filament fabrication (FFF) processed PLA, ABS, PETG, PA6, and PP thermoplastic polymers. *Polymers*. 2020;12(12):2924. doi:10.3390/polym12122924
22. Rodzeń K, Harkin-Jones E, Wegrzyn M, Sharma PK, Zhigunov A. Improvement of the layer-layer adhesion in FFF 3D printed PEEK/carbon fibre composites. *Compos A: Appl Sci Manuf*. 2021;149:106532. doi:10.1016/j.compositesa.2021.106532
23. Chicos LA, Pop MA, Zaharia S-M, et al. Fused filament fabrication of short glass fiber-reinforced polylactic acid composites: infill density influence on mechanical and thermal properties. *Polymers*. 2022;14(22):4988. doi:10.3390/polym14224988
24. Ergene B, Atlıhan G, Pinar A. Experimental and finite element analyses on the vibration behavior of 3D-printed PET-G tapered beams with fused filament fabrication. *Multidiscip Model Mater Struct*. 2023;19:19-651. doi:10.1108/MMMS-11-2022-0265
25. Li N, Li Y, Liu S. Rapid prototyping of continuous carbon fiber reinforced polylactic acid composites by 3D printing. *J Mater Process Technol*. 2016;238:218-225. doi:10.1016/j.jmatprotec.2016.07.025
26. Bolat Ç, Ergene B, Ispartalı H. A comparative analysis of the effect of post-production treatments and layer thickness on tensile and impact properties of additively manufactured polymers. *Int Polym Process*. 2023;38(2):244-256. doi:10.1515/ipp-2022-4267
27. Kallel A, Koutiri I, Babaeitorkamani E, et al. Study of bonding formation between the filaments of PLA in FFF process. *Int Polym Process*. 2019;34:434-444. doi:10.3139/217.3718
28. Sakthivel A, Muthukumaran E, Kandasamy J. A case study of 3D printed PLA and its mechanical properties. *Mater Today Proceed*. 2018;5:11219-11226. doi:10.1016/j.matpr.2018.01.146
29. Vidakis N, Petousis M, Savvakis K, Maniadi A, Koudoumas E. A comprehensive investigation of the mechanical behavior and the dielectrics of pure polylactic acid (PLA) and PLA with graphene (GnP) in fused deposition modeling (FDM). *Int J Plast Technol*. 2019;23:195-206. doi:10.1007/s12588-019-09248-1
30. Leonés A, Sonseca A, López D, Fiori S, Peponi L. Shape memory effect on electrospun PLA-based fibers tailoring their thermal response. *Eur Polym J*. 2019;117:217-226. doi:10.1016/j.eurpolymj.2019.05.010
31. Ehrmann G, Ehrmann A. Investigation of the shape-memory properties of 3D printed PLA structures with different infills. *Polymers*. 2021;13(1):164. doi:10.3390/polym13010164
32. Mathijsen D. Now is the time to make the change from metal to composites in naval shipbuilding. *Reinf Plast*. 2016;60:60-293. doi:10.1016/j.repl.2016.08.003
33. Tawfik BE, Leheta H, Elhewy A, Elsayed T. Weight reduction and strengthening of marine hatch covers by using composite materials. *Int J Naval Archit Ocean Eng*. 2017;9(2):185-198. doi:10.1016/j.ijnaoe.2016.09.005
34. Gargano A, Pingkarawat K, Blacklock M, Pickerd V, Mouritz AP. Comparative assessment of the explosive blast performance of carbon and glass fibre-polymer composites used in naval ship structures. *Compos Struct*. 2017;171:306-316. doi:10.1016/j.compstruct.2017.03.041
35. Dou H, Cheng Y, Ye W, et al. Effect of process parameters on tensile mechanical properties of 3D printing continuous carbon fiber-reinforced PLA composites. *Materials*. 2020;13(17):3850. doi:10.3390/ma13173850
36. Bochnia J, Blasiak M, Kozior T. A comparative study of the mechanical properties of FDM 3D prints made of PLA and carbon fiber-reinforced PLA for thin-walled applications. *Materials*. 2021;14(22):7062. doi:10.3390/ma14227062
37. Heidari-Rarani M, Rafiee-Afarani M, Zahedi AM. Mechanical characterization of FDM 3D printing of continuous carbon fiber reinforced PLA composites. *Compos Part B Eng*. 2019;175:107147. doi:10.1016/j.compositesb.2019.107147
38. Gavali VC, Kubade PR, Kulkarni HB. Mechanical and thermo-mechanical properties of carbon fiber reinforced thermoplastic composite fabricated using fused deposition modeling method. *Mater Today Proceed*. 2020;22(Part 4):1786-1795:1786-1795. doi:10.1016/j.matpr.2020.03.012
39. Kamaal M, Anas M, Rastogi H, Bhardwaj N, Rahaman A. Effect of FDM process parameters on mechanical properties of 3D-printed carbon fibre–PLA composite. *Prog Addit Manuf*. 2021;6:63-69. doi:10.1007/s40964-020-00145-3
40. Magri AE, El Mabrouk K, Vaudreuil S, Touhami ME. Mechanical properties of CF-reinforced PLA parts manufactured by fused deposition modeling. *J Thermoplast Compos Mater*. 2021;34(5):581-595. doi:10.1177/0892705719847244
41. Srinivasan R, Aravindkumar N, Aravind Krishna S, Aadhishwaran S, George J. Influence of fused deposition modelling process parameters on wear strength of carbon fibre PLA. *Mater Today Proceed*. 2020;27(Part 2):1794-1800:1794-1800. doi:10.1016/j.matpr.2020.03.738
42. Mohamed OA, Masood SH, Bhowmik JL. Analysis of wear behavior of additively manufactured PC-ABS parts. *Mater Lett*. 2018;230:261-265. doi:10.1016/j.matlet.2018.07.139
43. Al Abir A, Chakrabarti D, Trindade B. Fused filament fabricated poly(lactic acid) parts reinforced with short carbon fiber and graphene nanoparticles with improved tribological properties. *Polymers*. 2023;15(11):2451. doi:10.3390/polym15112451
44. Hanon MM, Zsidai L. Comprehending the role of process parameters and filament color on the structure and tribological performance of 3D printed PLA. *J Mater Res Technol*. 2021;15:647-660. doi:10.1016/j.jmrt.2021.08.061
45. Şirin Ş, Aslan E, Akincioğlu G. Effects of 3D-printed PLA material with different filling densities on coefficient of friction performance. *Rapid Prototyp J*. 2023;29(1):157-165. doi:10.1108/RPJ-03-2022-0081
46. ASTM G99. Standard Test Method for Wear and Friction Testing with a Pin-on-Disk or Ball-on-Disk Apparatus. https://www.astm.org/standards/g99, Last Access date: 18.04.2024
47. Flashforge, Filaments. https://flashforge.com/collections/filament, Last Access date: 31.07.2024
48. Hanon MM, Zsidai L, Ma Q. Accuracy investigation of 3D printed PLA with various process parameters and different colours. *Mater Today: Proc*. 2021;42(5):3089-3096. doi:10.1016/j.matpr.2020.12.1246
49. Bolat Ç, Ergene B. Wear performance of short fiber added polyamide composites produced by additive manufacturing:

combined impacts of secondary heat treatment, reinforcement type, and test force. *Polym Compos*. 2024;45:6885-6900. doi:10.1002/pc.28236

50. Jain R, Nauriyal S, Gupta V, Khas KS. Effects of process parameters on surface roughness, dimensional accuracy and printing time in 3D printing. In: Pandey PM, Kumar P, Sharma V, eds. *Advances in Production and Industrial Engineering*. Lecture Notes in Mechanical Engineering. Springer; 2021. doi:10.1007/978-981-15-5519-0_15
51. Bilkar D, Keshavamurthy R, Tambrallimath V. Influence of carbon nanofiber reinforcement on mechanical properties of polymer composites developed by FDM. *Mater Today: Proc*. 2020;46:4559-4562. doi:10.1016/j.matpr.2020.09.707
52. Ecker JV, Haider A, Burzic I, Huber A, Eder G, Hild S. Mechanical properties and water absorption behaviour of PLA and PLA/wood composites prepared by 3D printing and injection moulding. *Rapid Prototyp J*. 2019;25:672-678. doi:10.1108/rpj-06-2018-0149
53. Moreno Nieto D, Alonso-García M, Pardo-Vicente M-A, Rodríguez-Parada L. Product design by additive manufacturing for water environments: study of degradation and absorption behavior of PLA and PETG. *Polymers*. 2021;13(7):1036. doi:10.3390/polym13071036
54. Dhakal HN, Zhang ZY, Richardson MOW. Effect of water absorption on the mechanical properties of hemp fibre reinforced unsaturated polyester composites. *Compos Sci Technol*. 2007;67(7–8):1674-1683. doi:10.1016/j.compscitech.2006.06.019
55. Guo G, Finkenstadt VL, Nimmagadda Y. Mechanical properties and water absorption behavior of injection-molded wood fiber/carbon fiber high-density polyethylene hybrid composites. *Adv Compos Hybrid Mater*. 2019;2:690-700. doi:10.1007/s42114-019-00116-5
56. Chandran V, Kalman J, Fayazbakhsh K, Bougherara H. A comparative study of the tensile properties of compression molded and 3D printed PLA specimens in dry and water saturated conditions. *J Mech Sci Technol*. 2021;35(5):1977-1985. doi:10.1007/s12206-021-0415-5
57. Ergene B, Bolat Ç. An experimental study on the role of manufacturing parameters on the dry sliding wear performance of additively manufactured PETG. *Int Polym Process J Polym Process Soc*. 2022;37:37-270. doi:10.1515/ipp-2022-0015

SUPPORTING INFORMATION

Additional supporting information can be found online in the Supporting Information section at the end of this article.

How to cite this article: Ergene B, İnci YE, Çetintaş B, Daysal B. An experimental study on the wear performance of 3D printed polylactic acid and carbon fiber reinforced polylactic acid parts: Effect of infill rate and water absorption time. *Polym Compos*. 2024;1-15. doi:10.1002/pc.28993